© 2021. Published by The Company of Biologists Ltd | Journal of Cell Science (2021) 134, jcs248294. doi:10.1242/jcs.248294

RESEARCH ARTICLE

Distinct epithelial-to-mesenchymal transitions induced by *PIK3CA*^{H1047R} and *PIK3CB*

Ersa Gjelaj and Paul A. Hamel*

ABSTRACT

The most common *PIK3CA* mutation, producing the H1047R mutant of p110α, arises in myriad malignancies and is typically observed in low-grade breast tumours. In contrast, amplification is observed for wild-type *PIK3CB*, encoding p110β, and occurs at low frequency but in aggressive, high-grade metastatic tumours. We hypothesized that mutant p110α^{H1047R} and wild-type p110β give rise to distinct transformed phenotypes. We show that p110α^{H1047R} and wild-type p110β, but not wild-type p110α, transform MCF-10A cells and constitutively stimulate phosphoinositide 3-kinase (PI3K)-AKT pathway signalling. However, their resultant morphological transformed phenotypes are distinct. p110α^{H1047R} induced an epithelial-to-mesenchymal transition (EMT) commensurate with SNAIL (also known as SNAI1) induction and loss of E-cadherin. Upon p110β expression, however, E-cadherin expression was maintained despite cells readily delaminating from epithelial sheets. Distinct from the prominent filopodia in p110α^{H1047R}-expressing cells, p110β induced formation of lamellipodia, and these cells migrated with significantly greater velocity and decreased directionality. p110β-induced phenotypic alterations were accompanied by hyperactivation of RAC1; the dependency of transformation of p110β-binding to Rac1 revealed using a Rac1-binding mutant of p110β. Thus, *PIK3CB* amplification induces a transformed phenotype that is dependent upon a p110β-Rac1 signalling loop and is distinct from the transformed phenotype induced by p110α^{H1047R}.

KEY WORDS: PI3K, PIK3CB, Rac1, Epithelial-to-mesenchymal transition, Mammary epithelial cells, Migration

INTRODUCTION

Aberrant activation of phosphoinositide 3-kinase (PI3K) signalling occurs in up to 42% of breast tumours (Cancer Genome Atlas Network, 2012; Pereira et al., 2016). The PI3K signalling cascade is dependent on an evolutionarily conserved family of enzymes, PI3Ks, that are divided into classes based on their structure and functional properties (Thorpe et al., 2015; Vanhaesebroeck et al., 1997). Class IA PI3Ks are obligate heterodimers, consisting of a catalytic subunit (p110α, p110β or p110δ; encoded by *PIK3CA*, *PIK3CB* and *PIK3CD*, respectively), and a regulatory subunit (p85α, p85β, p50α, p55α or p55γ; with p85α, p50α and p55α encoded by *PIK3R1*, p85β by *PIK3R2*, and p55γ by *PIK3R3*) that harbor an N-terminal and C-terminal Src homology-2 (SH2) domains (Shibasaki et al., 1991; Vanhaesebroeck et al., 1997). Of these PI3Ks, p110α and p110β are ubiquitously expressed in all tissues, whereas p110δ appears restricted to cells of the immune system (Bi et al., 1999, 2002). Activation of PI3K signalling is observed in response to a variety of cellular ligands while, in resting cells, repression of signalling occurs through a p85 subunit binding to a p110 subunit and inhibiting its activity. This inhibition is mediated by the C2–iSH2 interface between p110 and p85 (Zhang et al., 2011). Ligand-dependent stimulation of receptor tyrosine kinases (RTKs) recruits PI3K to the membrane through p85 docking to activated RTKs (Kazlauskas, 1994; Pawson et al., 1993; Vanhaesebroeck et al., 1997). This interaction alleviates inhibition of the p110 catalytic subunit, allowing for phosphorylation of its lipid substrate phosphoinositide-(4,5)-bisphosphate (PIP2) producing the secondary lipid messenger phosphoinositide-(3,4,5)-triphosphate (PIP3) (Downes and Carter, 1991). In contrast to p110α, p110β has unique, non-redundant functions and is activated downstream of G-protein-coupled receptors (GPCRs), through direct interaction with Gβγ subunits, independently of its inhibition by p85 (Dbouk et al., 2012; Guillermet-Guibert et al., 2008). Indeed, p110β is dispensable for RTK-mediated activation of PI3K signalling due, at least in part, to the disrupted C2–iSH2 interface between wild-type p110β and p85. Recruitment of PI3K isoforms to the membrane and production of PIP3 subsequently signals through additional downstream factors in this pathway. One of the most well-characterized effectors of PI3K signalling are the serine/threonine AKT protein kinase family (AKT1–AKT3, hereafter generically referred to as AKT). Recruitment of AKT to the plasma membrane occurs through binding of its pleckstrin homology (PH) domain to PIP3 (Coffer et al., 1998). Phosphorylation and activation of AKT, in turn, phosphorylates and activates numerous targets that regulate myriad cellular processes (for a review, see Manning and Toker, 2017).

Although initially thought to be functionally redundant owing to their similar structural domains, substrates and lipid products (Singh et al., 2016), p110α and p110β have distinct activities and roles in breast cancer (Utermark et al., 2012). *PIK3CA*, encoding the p110α protein, is mutated at high frequency in breast cancers. Predominant transforming mutations are evident for three 'hot-spots' within the helical (E542K, E545K) and kinase (H1047R) domains of p110α (Samuels and Velculescu, 2004). This latter variant is the most frequent mutation in p110α in breast cancer (Pereira et al., 2016) and is also observed at high frequency in many other neoplasms (Hoadley et al., 2014). These oncogenic variants arise due to missense mutations that generate constitutively active variants of p110α (Gabelli et al., 2010; Isakoff et al., 2005). In contrast, hot-spot mutations in *PIK3CB*, encoding the p110β protein, are essentially absent in breast tumours. However, amplification of *PIK3CB* does occur in 1.4–1.6% of breast cancers (Cancer Genome Atlas Research Network et al., 2013b) and at considerably higher frequency in a number of other neoplasms, including lung squamous cell carcinoma (12–18%; Cancer Genome Atlas Research Network, 2012; Hoadley et al., 2018), ovary serous cystadenocarcinoma (5–12%; Cancer Genome Atlas Research Network, 2011; Hoadley et al., 2018),

Department of Laboratory Medicine & Pathobiology, Faculty of Medicine, University of Toronto, Toronto, ON M5S 1A8, Canada.

*Author for correspondence (paul.hamel@utoronto.ca)

P.A.H., 0000-0002-3844-8850

Handling Editor: Kathleen Green
Received 30 April 2020; Accepted 13 January 2021

Journal of Cell Science (2021) 134, jcs248294. doi:10.1242/jcs.248294

uterine corpus endometrial carcinoma (8–11%; Cancer Genome Atlas Research Network et al., 2013a; Hoadley et al., 2018), head and neck squamous carcinoma (9%; Hoadley et al., 2018) and cervical squamous cell (8%; Hoadley et al., 2018). Unlike p110α, which requires activating mutations to acquire its oncogenic properties, wild-type p110β can induce transformation of cultured cells due, in part, to its disrupted C2–iSH2 interface with p85β (Dbouk et al., 2010; Kang et al., 2006). In p110α, its interaction with p85 is mediated by N345 which interacts with D560 and N564 in p85. The activating N345K point mutation in p110α results in decreased inhibition by p85. Interestingly, for p110β, the amino acid residue K342 aligns with N345 residue in p110α. Thus, wild-type p110β is analogous to the oncogenic N345K variant of p110α, both being minimally inhibited by the p85 regulatory partners (Dbouk et al., 2010). Indeed, physiological levels of wild-type p110β are sufficient and necessary for tumour growth and survival in a PTEN-deficient tumour xenograft model, consistent with a role for wild-type p110β as an oncoprotein (Wee et al., 2008). p110β also contributes to the growth of ErbB2-dependent mammary tumours (Ciraolo et al., 2008). p110β elicits its oncogenic properties through interaction with Rac1 and Cdc42, members of the Rho-family GTPases (Fritsch et al., 2013). Mice harbouring point mutations in key residues (S205D and K224D) in the Ras-binding domain (RBD) of p110β reduce its PI3K activity but also reveal the requirement for Rac1 and Cdc42 in regulation of p110β activity *in vivo* (Fritsch et al., 2013).

The unique dependency on Rho GTPases, specifically Rac1, for p110β activity in tumour models suggested that p110β-mediated PI3K signalling may elicit distinct cytoskeletal and molecular phenotype relative to cells transformed by the predominant transforming variant of *PIK3CA*, p110α^{H1047R}. We show here that MCF-10A human mammary epithelial cells expressing wild-type p110β have a phenotype that is distinct from MCF-10A cells transformed due to expression of p110α^{H1047R}. Expression of p110β and the p110α^{H1047R} mutant both constitutively activate AKT. However, the epithelial-to-mesenchymal transition (EMT) elicited by p110α^{H1047R} operates through induction of SNAIL (also known as SNAI1) and the commensurate loss of E-cadherin. In contrast, p110β expression produces a distinct phenotype where cells exhibited enhanced motility and invasive properties but not the loss of epithelial markers characteristic of EMT. Finally, we show that the phenotype induced by p110β is dependent on the interaction between p110β and Rac1.

RESULTS

Constitutive activation of AKT by p110α^{H1047R} or wild-type p110β in mammary epithelial cells

In a recent paper, p110α^{H1047R}- or wild-type p110β-dependent transformation of MCF-10A cells was determined to induce activation YAP and TAZ through multiple signalling pathways (Zhao et al., 2018). Employing these cells, we first determined whether stable overexpression of p110β resulted in similar constitutive activation of PI3K signalling as is seen following expression of p110α^{H1047R} (Isakoff et al., 2005). Stable expression of MCF-10A cells expressing wild-type p110α, p110α^{H1047R} or wild-type p110β was confirmed via western blotting (Fig. 1A). Furthermore, relative mRNA expression of wild-type *PIK3CA* and *PIK3CA*^{H1047R} were confirmed via amplification of the HA tag and N-terminal region of *PIK3CA* (Fig. 1B). Normalized relative expression of total *PIK3CA* and *PIK3CB* expression was also determined across all MCF-10A cell lines (Fig. 1B). Transcript levels of HA-tagged *PIK3CA* were higher (overexpressed) relative to parental and p110β-expressing MCF-10A cells, and comprised the total *PIK3CA* transcript (Fig. 1B). Furthermore, *PIK3CB* was overexpressed in p110β-expressing MCF-10A cells, but not in the other cell lines (Fig. 1B). Thus, the transcript levels of *PIK3CA* and *PIK3CB* coincided with the observed protein expression of these isoforms. PI3K signalling was then assessed in these cells by quantifying the level of phospho-Ser^{473} of AKT (denoted pAKT or pAKT^{S473}, with the antibody used detecting this residue in all AKT isoforms) (Fig. 1C). When cells are maintained in normal growth conditions (in the presence of EGF and insulin), high basal AKT activity was evident in cells expressing p110α^{H1047R} or wild-type p110β, relative to parental MCF-10A cells, or cells expressing wild-type p110α. Phosphorylation of AKT persisted upon growth factor withdrawal of EGF and insulin in cells expressing p110α^{H1047R} or wild-type p110β, while in parental MCF-10A cells or cells overexpressing wild-type p110α, the levels of activated AKT gradually diminished. To determine whether pAKT levels were maximal in p110α^{H1047R}- and p110β-expressing cells, the sensitivity of these lines to growth factor stimulation was evaluated (Fig. 1D). Dose-dependent activation by EGF of AKT was apparent for cells expressing wild-type p110α and parental MCF-10A lines. In contrast, no further increase in pAKT levels was seen for p110α^{H1047R}- and p110β-expressing cells. The dependence of AKT activation on the activity of p110α^{H1047R} or p110β was verified by repressing their activity with the PI3K inhibitor, Wortmannin. Phosphorylation at Ser^{473} of AKT was abolished at all concentrations of Wortmannin (Fig. 1E). Thus, both p110α^{H1047R} and p110β stimulate the PI3K signalling pathway by constitutively activating AKT in MCF-10A cells, analogous to their similar stimulation of YAP/TAZ signalling (Zhao et al., 2018).

p110α^{H1047R} and p110β invoke distinct phenotypes in MCF-10A cells

Wild-type p110α does not constitutively activate PI3K signalling and has no apparent morphological effects when expressed in MCF-10A cells relative to control MCF-10A, as shown previously (Isakoff et al., 2005) (Fig. 2A). However, as is evident in Fig. 2A, ectopic expression of p110α^{H1047R} or wild-type p110β produced profound but distinct morphological alterations in MCF-10A cells. For both p110α^{H1047R} and wild-type p110β, an apparent EMT was evident. For p110α^{H1047R}, cells acquired a spindle-like morphology, resembling fibroblasts, and often exhibited elongated filopodia. In contrast, while undergoing an apparent EMT, MCF-10A cells expressing wild-type p110β exhibited a phenotype distinct from p110α^{H1047R}-expressing cells. Specifically, p110β-expressing cells had a flattened appearance and extensive lamellipodia, which are characteristic of migrating cells, and were apparently larger in overall size in 2D cultures (Fig. 2A).

The dependency of the altered phenotype on p110α^{H1047R} and p110β, respectively, was revealed using the PI3K-inhibitor Wortmannin (Fig. 2B,C). Cells seeded onto coverslips were treated with Wortmannin and stained with phalloidin (Fig. 2B) or for β-catenin (Fig. 2C). Upon inhibition of MCF-10A cells expressing p110α^{H1047R} or p110β with Wortmannin, cells reverted to the morphology characteristic of epithelial cells. Furthermore, actin stress fibres, typically observed in mesenchymal cells to assist with migration (for a review, see Tojkander et al., 2012), are apparent in p110α^{H1047R}- and p110β-expressing cells and disappear upon inhibition with Wortmannin. Rather, phalloidin staining reveals a cortical actin belt within these cells characteristic of epithelial cellular morphology. Additionally, cells became more rounded and made close contacts with neighbouring cells. For the case of p110β, the significant lamellipodia evident for DMSO-treated cells were lost in cells treated with Wortmannin, illustrating the dependence of the significant phenotypic changes on p110β activity.

Journal of Cell Science (2021) 134, jcs248294. doi:10.1242/jcs.248294

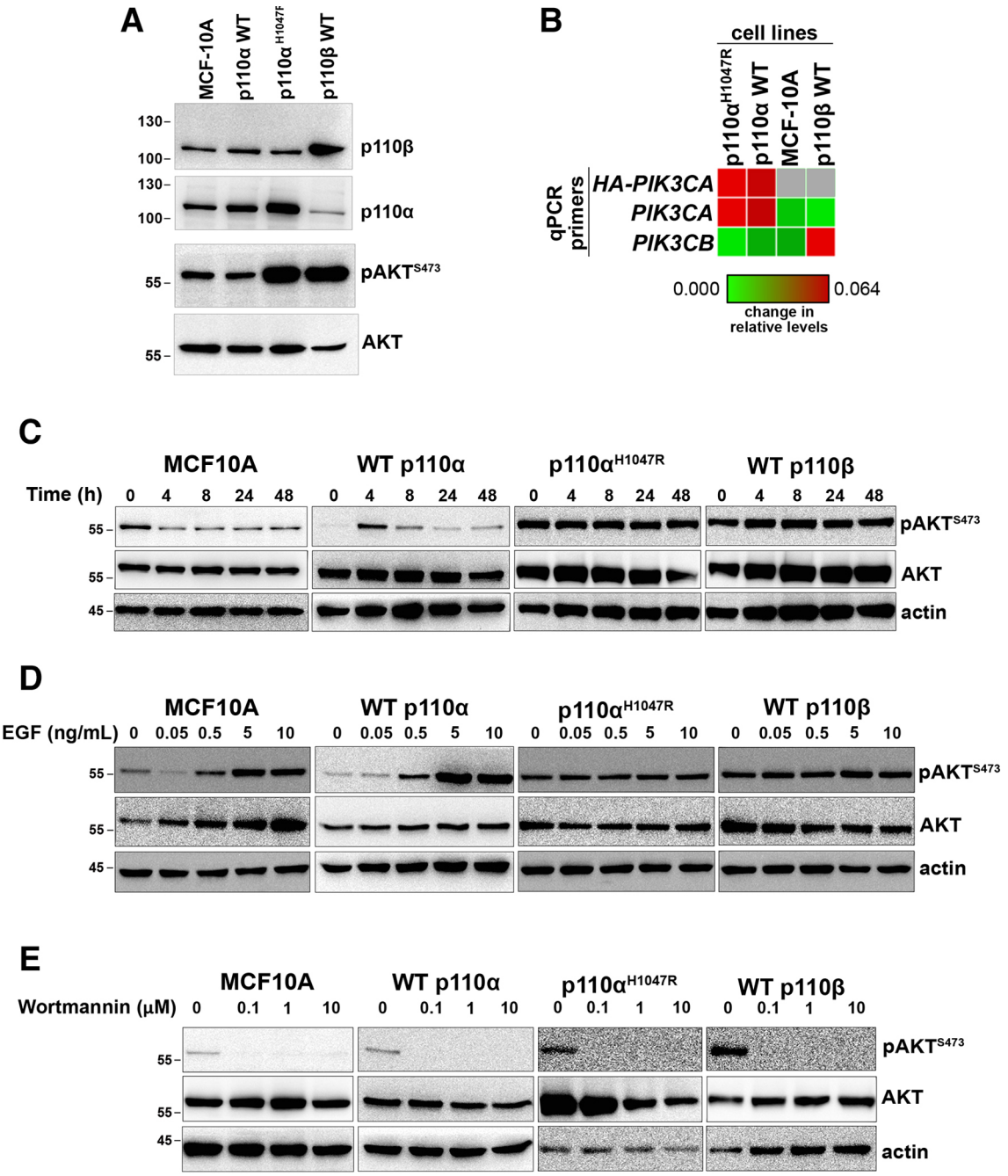

Fig. 1. Expression of p110α^{H1047R} and p110β, but not wild-type p110α, in MCF-10A cells cause constitutive activation AKT. (A,C–E) Representative western blot images depicting activation of the PI3K-AKT signalling pathway as shown by phosphorylation of AKT on Ser473 (pAKT^{S437}). (A) Levels of p110α and p110β in parent MCF-10A cells as well as cells expressing wild-type (WT) p110α, p110α^{H1047R} and p110β. Increased levels of pAKT^{S437} are only seen for p110α^{H1047R}- and p110β-expressing cells. (B) Relative levels of *HA-PIK3CA*, *PIK3CA* and *PIK3CB* in the different cultures determined by qPCR. (C) Growth factors (EGF and insulin) were withdrawn from MCF-10A culture medium over 48 h. Cells were (D) stimulated with increasing doses of EGF for 10 min following 24 h of growth factor withdrawal, or (E) inhibited with increasing doses of Wortmannin for 1 h.

Apicobasal polarity of epithelial cells due to the presence of cell–cell adhesion complexes at lateral membranes is lost as cells undergo EMT. As expected, MCF-10A cells had the expected distribution of E-cadherin and β-catenin at cell–cell contacts while p110α^{H1047R}-expressing cells exhibited a substantial reduction in E-cadherin (Fig. 3A) (Feigin and Muthuswamy, 2009; Huang et al., 2012; Knights et al., 2012; Le Bras et al., 2012; Macara and McCaffrey, 2013). Curiously, little decrease in E-cadherin staining was evident at lateral membranes in p110β-overexpressing MCF-10A cells in high confluency cultures (Fig. 3A). However, p110β-overexpressing MCF-10A cells also exhibited increased cytoplasmic localization of E-cadherin. These differences in E-cadherin and β-catenin expression were confirmed by western blot analysis (Fig. 3B,C).

The transcriptional repressor of E-cadherin, SNAIL, is activated when localized to the nucleus (Lamouille et al., 2014; Muqbil et al., 2014; Nieto, 2002; Zhou et al., 2004). Therefore, the protein level and localization of SNAIL was assessed. As Fig. 4A shows, SNAIL expression was induced only in cells expressing p110α^{H1047R}.

Journal of Cell Science (2021) 134, jcs248294. doi:10.1242/jcs.248294

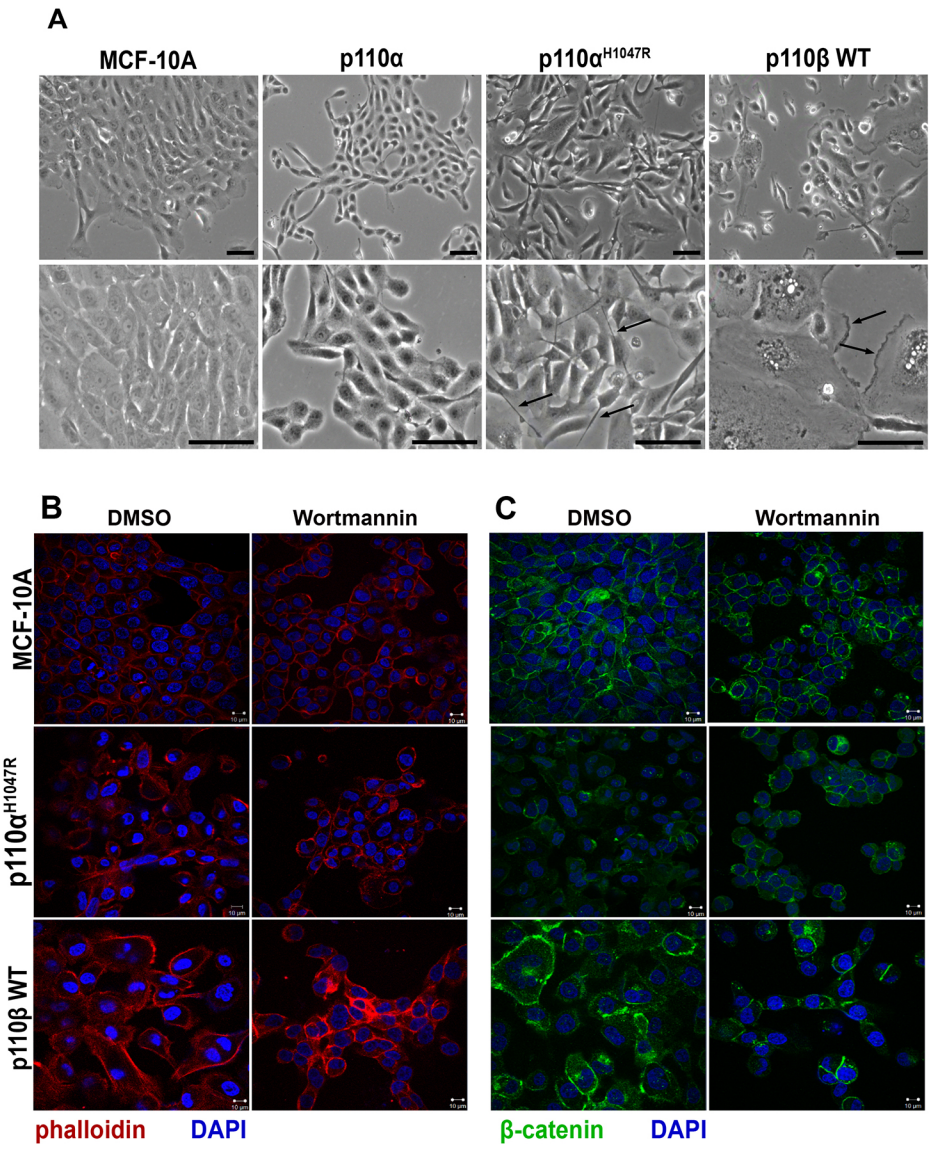

Fig. 2. Expression of the p110α^{H1047R} and p110β, respectively, induce distinct EMT-like phenotypes in MCF-10A cells. (A) Representative bright-field images of cell lines at mid-confluency. Parental MCF-10A cells and MCF-10A overexpressing p110α cells have a characteristic epithelial morphology. MCF-10A cells expressing p110α^{H1047R} acquire a spindle morphology with elongated filipodia (indicated by arrows), while p110β cells have enhanced cell spreading and produce extensive lamellipodia (indicated by arrows). Scale bars: 200 µm. Cells were plated on basement membrane extract and treated with DMSO or 100 nM Wortmannin for 4 h prior to staining for (B) phalloidin (TRITC) and (C) β-catenin (FITC) to assess the dependency of the EMT phenotype on PI3K. Representative confocal images depict (B) parental MCF-10A cells express cortical actin, while p110α^{H1047R} cells are more elongated and p110β cells have enhanced cell spreading; inhibition with Wortmannin results in circumferential localization of actin and decreases cell spreading with tighter cell–cell junctions. (C) Wortmannin enhances the expression of β-catenin at lateral membranes of neighbouring cells in both p110α^{H1047R}- and p110β-expressing MCF-10A cells, resembling more closely the morphology of the parental MCF-10A cells. Scale bars: 10 µm.

Likewise, p110α^{H1047R}-expressing cells, but not p110β-expressing cells, had strong induction of transcripts for *SNAI1* and the EMT marker *CDH2* (encoding N-cadherin) (Fig. 4B). Nuclear localization of SNAIL in p110α^{H1047R}-expressing cells was confirmed by western blotting following cell fractionation (Fig. 4C). Immunofluorescence staining revealed further that SNAIL accumulates in the nucleus of p110α^{H1047R}-expressing cells (see yellow arrows in Fig. 4D) and, in the same culture where SNAIL expression is apparently absent in the occasional cell, membrane expression of E-cadherin is observed (red arrows, Fig. 4D).

The decreased expression of E-cadherin at cell–cell contacts in p110α^{H1047R}- and p110β- expressing lines suggested loss of apicobasal polarity in these cells. To characterize altered polarity, cells were plated on Matrigel and grown in 3D culture to form acini (Fig. 5A,B). The parent MCF-10A line formed acini with highly polarized cells. In contrast, both p110α^{H1047R}- and wild-type p110β-expressing cells formed large, dysmorphic acini. For both cell types, a hollow lumen was absent, indicating the apparent loss of cell polarity as well as a loss of apoptosis in luminal cells. The phenotype of p110β-expressing cells in 3D culture was, however, distinct from that of cells expressing p110α^{H1047R}. As the arrows in the bottom right panel in Fig. 5A, p110β expression caused the formation of invasive protrusions extending into the Matrigel bed. Furthermore, as is evident by the different scale bars, the overall size of these aggregates of cells were generally larger for p110β, consistent with their increased size evident in 2D cultures (see Fig. 2).

These data reveal that p110α^{H1047R} induces an apparent EMT through loss of E-cadherin and transcriptional induction of *SNAI1* while cells expressing wild-type p110β maintain E-cadherin expression but undergo loss of apicobasal polarity. Thus, despite both p110α^{H1047R} and p110β activating PI3K signalling through AKT, the morphology and transcriptional programme of the resultant cells are distinct.

p110β overexpression increases cellular motility

Epithelial cells migrate collectively owing to strong cell–cell contacts, which inhibits migration of single cells (Elisha et al., 2018; Larue and Bellacosa, 2005). Furthermore, directional migration is mediated by extension of lamellipodia from cells, which is dependent on polarization and restriction of lamellipodia to the leading front of the plasma membrane (Cain and Ridley, 2009; Ridley, 2015). To assess whether loss of cell–cell contacts, as well

Journal of Cell Science (2021) 134, jcs248294. doi:10.1242/jcs.248294

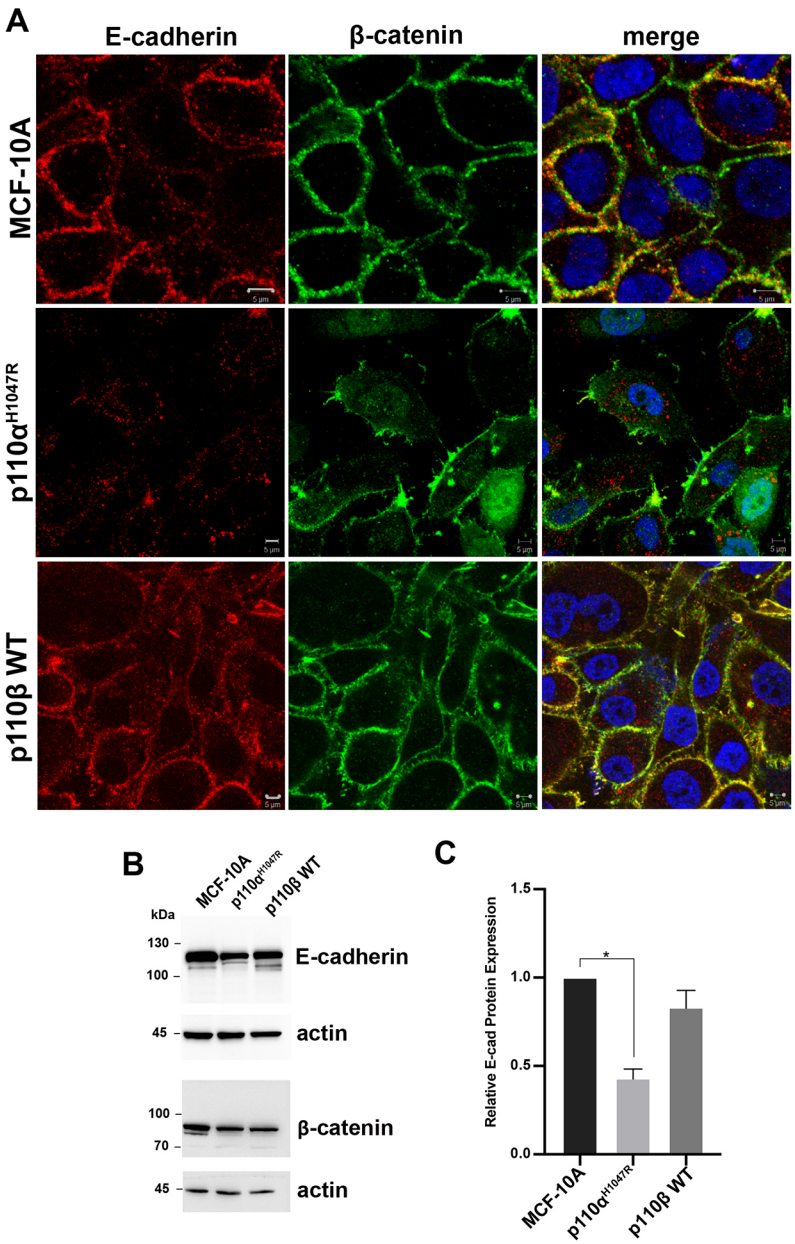

Fig. 3. Expression of p110α^{H1047R}, but not p110β, results in loss of E-cadherin protein expression at lateral membranes. (A) Cells were grown to confluency and representative confocal images show expression of E-cadherin and β-catenin at lateral membranes, nuclei were stained with DAPI. E-cadherin expression was substantially reduced in p110α^{H1047R} cells, but not in p110β cells. Scale bars: 5 µm (B) Reduction in E-cadherin protein levels, and slight loss of β-catenin in p110α^{H1047R} and 110β overexpressing MCF-10A cells was confirmed by western blotting; p110α^{H1047R}, but not p110β cells had significantly decreased expression of E-cadherin. Results are mean±s.e.m. of three independent experiments. *P<0.0332 (two-way ANOVA with Tukey's analysis).

as apicobasal polarization, affects directional cell migration in p110α^{H1047R}- and p110β-expressing cells, wound assays were employed (Fig. 6). As expected, MCF-10A cells migrate across the scratch as a sheet, and cells at the leading edge remaining attached to the cells behind them as the wound closes. In contrast, cells expressing p110α^{H1047R} or p110β at the edge of the wound delaminated from the bulk of cells and migrated as single cells into the acellular areas. (Fig. 6A). Furthermore, p110β-expressing cells had an increased rate of wound closure in comparison to both p110α^{H1047R} expressing- and parental MCF-10A cells (Fig. 6B). Fig. 6C shows further that, while MCF-10A cells at the edge of the wound extend lamellipodia and filopodia into the wound oriented towards the direction of migration, these same features in p110α^{H1047R}- and p110β-expressing cells are disoriented, suggesting a loss of directionality in migration of these cells. Thus, the cell directionality as well as the velocity of individual cells was measured in this assay. As Fig. 7 illustrates, MCF-10A cells exhibited a highly directional migration pattern. p110α^{H1047R} cells were more variable in directionality in their migration, and this feature was even more pronounced for p110β cells. These differences were reflected in the different velocities for these cells in the same cultures, the p110β-expressing cells exhibited significantly greater velocity than the parent or p110α^{H1047R} cells. Thus, despite the maintenance of E-cadherin expression in p110β-overexpressing MCF-10A cells, these cells delaminated from adjacent cells and migrated with significantly greater velocity but in a more random manner relative to both p110α^{H1047R}-expressing and parental MCF-10A cells. Taken together with the invasive phenotype of acini formed from p110β overexpressing MCF-10A cells in 3D culture, p110β overexpression gives rise to a distinct, highly motile phenotype.

Morphology and EMT induced by p110β is dependent on binding to and activation of Rac1

A unique activity of p110β is its interaction with Rho GTPases. The RBD of p110β binds Rac1 and Cdc42, and, Rac1 specifically is

Journal of Cell Science

Journal of Cell Science (2021) 134, jcs248294. doi:10.1242/jcs.248294

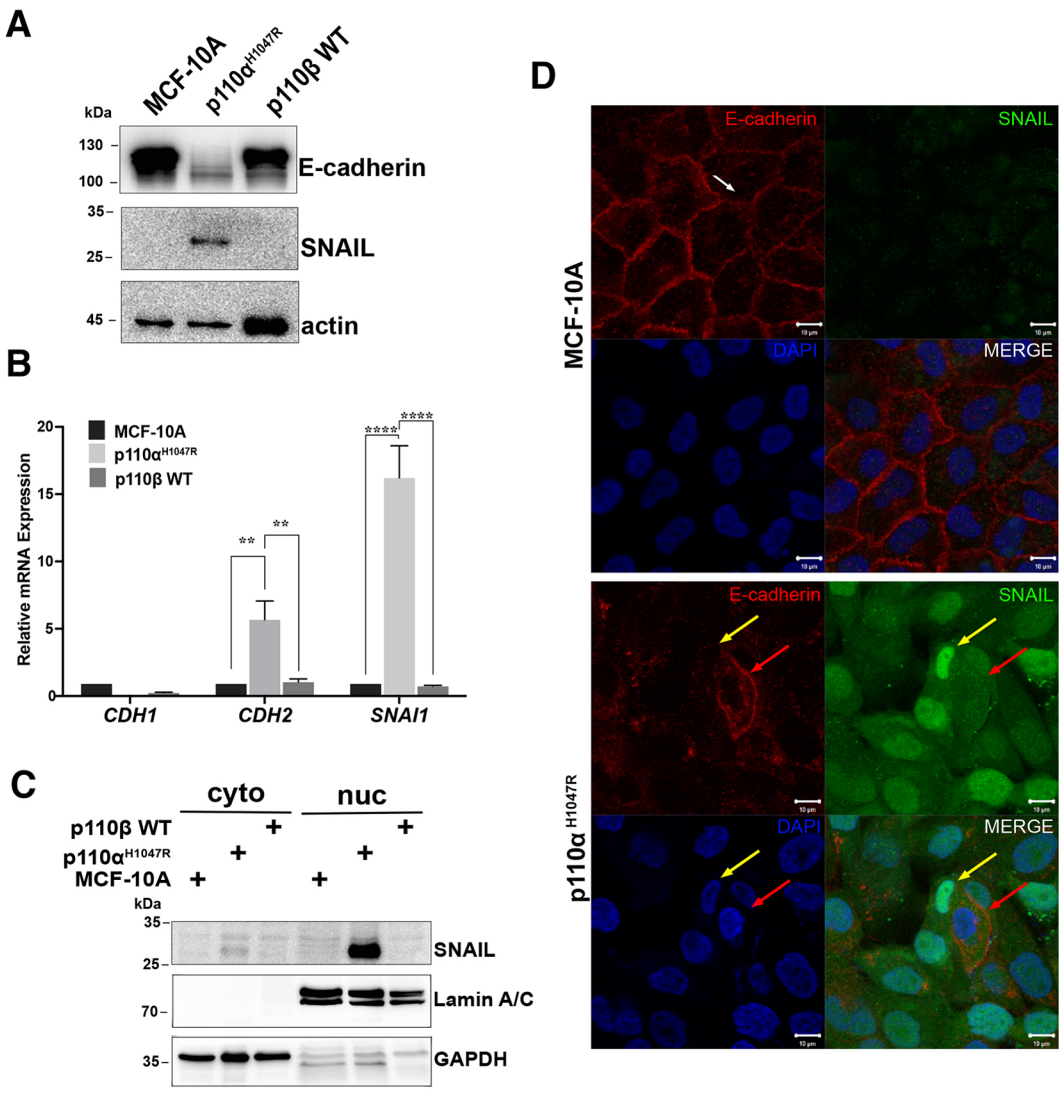

Fig. 4. p110α^{H1047R} expression induces expression and nuclear localization of SNAIL. (A) p110α^{H1047R} cells, but not p110β, had induction of SNAIL, concomitant with a reduction in E-cadherin protein expression, as depicted by a representative western blot image probed with indicated primary antibodies. (B) Induction of *SNAI1* transcript is evident in p110α^{H1047R} cells, as well as induction of the mesenchymal marker *CDH2* (N-cadherin), but not 110β cells, relative to parental MCF-10A cells. Results are representative of the mean±s.e.m. of three independent experiments. ***P*<0.0021, *****P*<0.0001 (two-way ANOVA with Tukey's analysis). (C) Representative western blot image of cytoplasmic (cyto) and nuclear (nuc) fractionation of cellular lysates, showing SNAIL localization in the nuclear fraction of p110α^{H1047R} cells. (D) Representative confocal images of p110α^{H1047R} cells showed nuclear localization of SNAIL and concomitant loss of E-cadherin at lateral membrane. Yellow arrows indicate a cell with high SNAIL expression but loss of E-cadherin while red arrows shows an adjacent cell with undetectable SNAIL commensurate with high E-cadherin at lateral membrane. Scale bars: 10 µm.

indispensable for functions of p110β in several cellular and murine models (Cizmecioglu et al., 2016; Fritsch et al., 2013; Yuzugullu et al., 2015; Zhang et al., 2017). Furthermore, Rac1 regulates lamellipodia formation and actin cytoskeleton remodelling (Nobes and Hall, 1994). Owing to the distinct morphological alterations in p110β-overexpressing cells, levels of activated Rac1 were determined. Cells expressing p110β uniquely increased levels of activated Rac1 relative to p110α^{H1047R} and the parental MCF-10A cells (Fig. 8A,B).

In order to determine the dependency of the phenotype produced by p110β-overexpression on activation of Rac1, S211D and K230A mutations (p110β$^{SD/KA}$; Fig. 8C), shown previously to prevent binding and activation of Rac1 (Fritsch et al., 2013), were introduced into the RBD of p110β. As shown in Fig. 8D, increasing levels of virus expressing the p110β$^{SD/KA}$ mutant gave rise to increased levels of p110β protein. For all levels of virus, increased pAKT was observed. However, these levels did not increase proportionately with the increased levels of p110β protein nor did they reach the levels determined for wild-type p110β. Fig. 8E shows further that cells expressing the highest levels of the p110β$^{SD/KA}$ mutant did not exhibit the apparent EMT evident for wild-type p110β. Rather, these cells maintained the morphology of the parental MCF-10A cells.

Thus, while p110α^{H1047R} causes an EMT in MCF-10A cells as well as induction of PI3K signalling through activated AKT, these data show in this model system of mammary epithelial cells that, despite activating the PI3K pathway through AKT, analogous to the transforming p110α^{H1047R} protein, wild-type p110β also operates through distinct pathways that depend on binding to Rac1. These distinct pathways generate a unique phenotype for the cells that includes a significant increase in the migratory behaviour of MCF-10A mammary epithelial cells.

Journal of Cell Science (2021) 134, jcs248294. doi:10.1242/jcs.248294

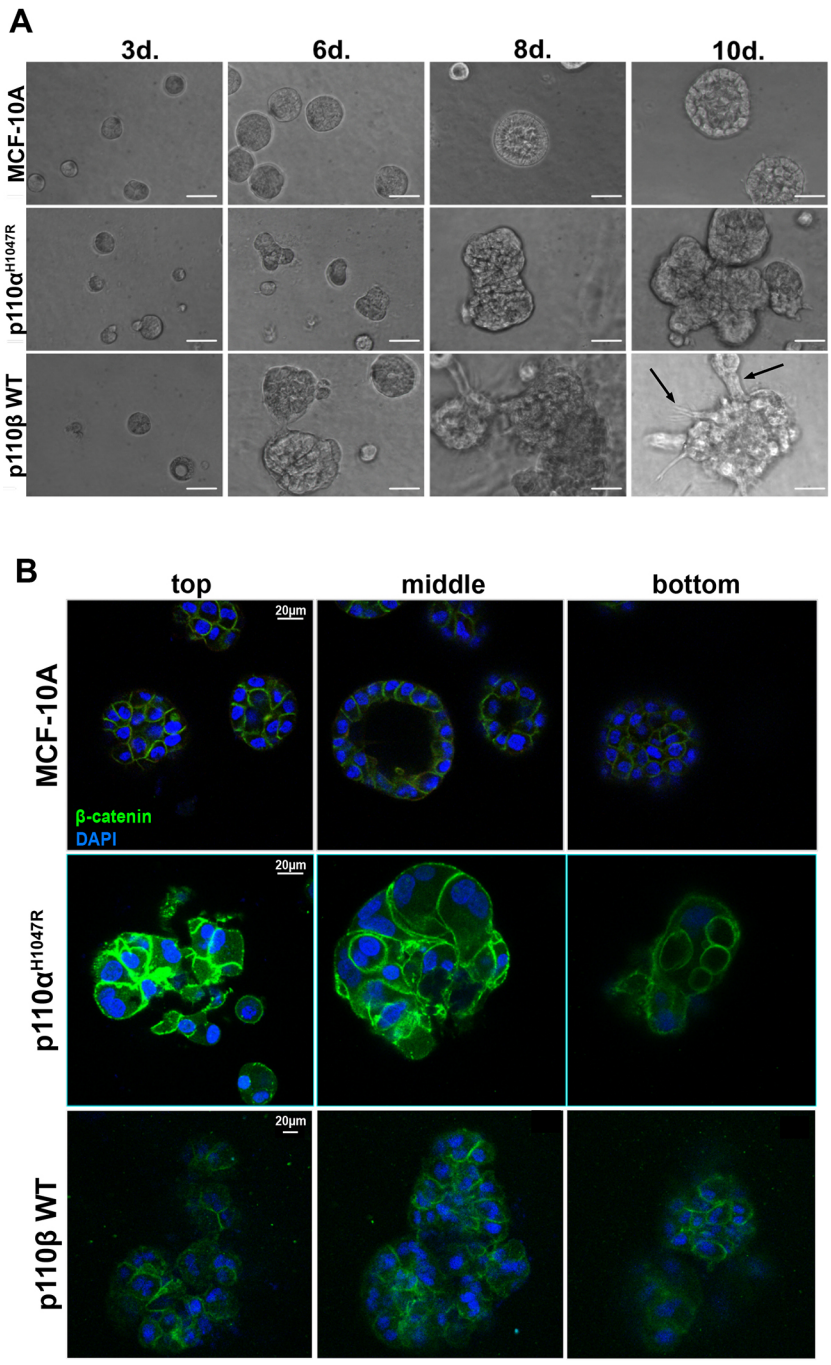

Fig. 5. Expression of p110α^{H1047R} and p110β in MCF-10A cells, respectively, form acini with loss of apicobasal polarization. MCF-10A cell lines were plated on Matrigel for 10–12 days in the presence of EGF. (A) Representative bright-field images of acini formed over 10 days. p110α^{H1047R} and p110β cells form large, dysmorphic acini. 110β overexpression induces the formation of invasive protrusions that extend into the Matrigel bed (depicted by arrows) Scale bars: 100 µm. (B) Representative confocal images demonstrating acini morphology, p110α^{H1047R} and p110β cells have apparent loss of apicobasal polarity, FITC indicates β-catenin at lateral membranes, nuclei stained with DAPI. Scale bars: 20 µm; note that the p110β image is half the size of other images due to the large size of cells in acini due to 110β expression.

DISCUSSION

The results presented here demonstrate that despite constitutive activation of the PI3K-AKT pathway downstream of both p110α and p110β, these isoforms give rise to distinct phenotypes when expressed in mammary epithelial cells. It is apparent that both these oncoproteins induced an altered cellular phenotype, loss of apicobasal polarization, and random single-cell migration. However, these differences occurred through alterations in distinct molecular pathways. Notably, expression of the transforming p110α^{H1047R} protein caused an EMT through induction of SNAIL and commensurate repression of E-cadherin expression, while the effect of overexpression of wild-type p110β requires its association with Rac1.

Our data also demonstrate that despite constitutive activation of AKT by both p110α^{H1047R} or p110β, the resultant molecular and phenotypic program in MCF-10A cells are distinct. It remains unresolved, however, how isoform-specific activation of distinct pathways downstream of PI3K/AKT signalling is mediated, although the unique activities of p110β are also relevant. Rac1 binding to p110β is necessary for localization of p110β to membrane rafts harbouring GPCRs and for its association to Gβγ in these complexes to activate signalling downstream of GPCRs (Cizmecioglu et al., 2016; Fritsch et al., 2013). Disruption of membrane raft integrity also negatively affected p110β-dependent growth of PTEN breast cancer cell lines. p110α does not reside in membrane raft regions, thus its activity downstream of RTKs is unaffected by the disruption of membrane raft integrity (Cizmecioglu et al., 2016). These data suggest that targeted localization to signalling domains of p110β by Rac1 may be

Journal of Cell Science (2021) 134, jcs248294. doi:10.1242/jcs.248294

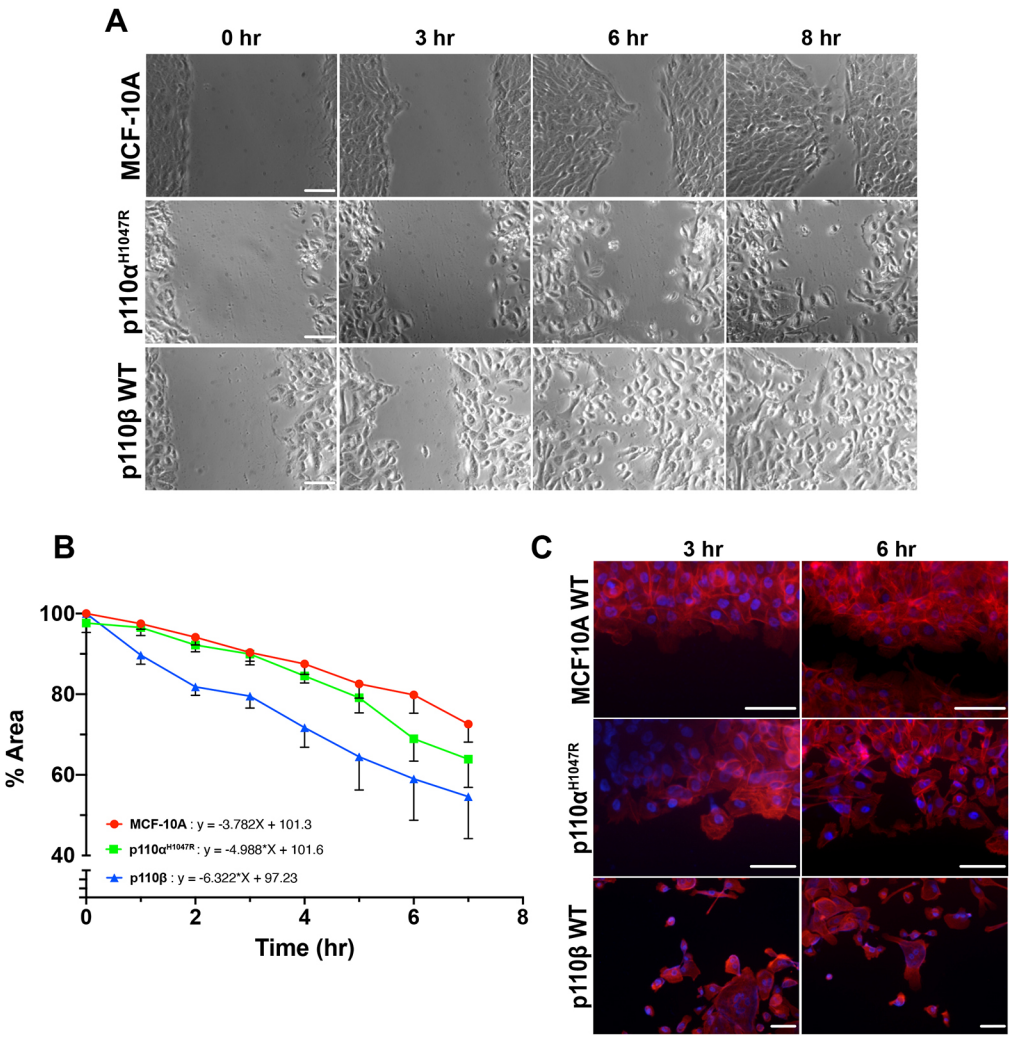

Fig. 6. p110β overexpression in MCF-10A cells invokes single cell migration. Cells were grown to confluency, a wound was scratched in the cell monolayer and cell migration was observed over 8 h. (A) Representative bright-field images of MCF-10A cell lines; p110β and p110α^{H1047R} cells migrate as single cells, p110β cells were able to fill wound in 8 h. Scale bars: 1000 µm. (B) The percentage of area of wound without cells over time was quantified. Curves were generated from three independent experiments for each cell line and show mean±s.e.m.; the equation fitting the slope of the graph is also given. (C) Representative fluorescence images of the leading edge of cells during migration; the actin cytoskeleton is depicted through phalloidin staining. p110β and p110α^{H1047R} cells lose front-to-rear polarity, and lamellipodia form at multiple regions of the plasma membrane. Scale bars: 50 µm.

integral to the transformative activities of p110β. Furthermore, the apparent heterogeneity we observed in PI3K-AKT signalling as a result of p110α^{H1047R} or p110β overexpression might be influenced by their localization to distinct membrane domains.

While Ras binding to p110α is necessary for maximal stimulation of PI3K signalling, the RBD of p110β binds Rac1 and Cdc42 (Fritsch et al., 2013). The Rho-family of GTPases play an important role in cytoskeleton reorganization, maintenance of cellular polarity, cell–cell adhesion and cell migration (Alan and Lundquist, 2013; Keely et al., 1997; Nobes and Hall, 1994; Ridley, 2004, 2015). Furthermore, dysregulation of these GTPases contributes to cancer cell migration, invasion and metastasis (Fritz et al., 1999, 2002). We observed significantly increased activation of Rac1 due to overexpression of p110β, but not the p110α^{H1047R} mutant. The resultant phenotype was enhanced cell spreading, extensive lamellipodia formation, increased motility and random migration of individual cells, which are consistent with the increased Rac1 activity. As shown previously, constitutively active Rac1 disrupts E-cadherin mediated cell–cell adhesion in subconfluent cultures (Akhtar and Hotchin, 2001). We observed a similar phenotype in MCF-10A cells expressing p110β in subconfluent cultures with cells exhibiting a mesenchymal phenotype lacking apparent cell–cell adhesions. Furthermore, Akhtar and Hotchin (2001) have shown that a constitutively active form of Rac1 induces endocytosis of E-cadherin leading to clathrin-independent internalization of E-cadherin and the formation of vesicles with colocalized Rac1 and E-cadherin. This observed role for Rac1 allows for dynamic turnover of E-cadherin at cell junctions and facilitates rapid delamination, and migration of epithelial cells. Indeed, we observed delamination of cells and random single cell migration in highly confluent cultures despite the presence of E-cadherin expression at cell–cell junctions in p110β-expressing cells. Furthermore, we observed increased cytoplasmic localization of E-cadherin in immunofluorescence images, relative to parental MCF-10A cells and MCF-10A cells expressing the p110α^{H1047R} mutant. These data suggest that constitutive activation of Rac1 in p110β-overexpressing MCF-10A cells might destabilize E-cadherin expression at adherens junctions thereby facilitating their motile phenotype. Furthermore, acini grown in 3D culture from p110β overexpressing MCF-10A cells had extensive invasive protrusions extending into the Matrigel bed. These protrusions were similar to those of mammary epithelial cells expressing constitutively active Rac1 and the Cdc42 guanine nucleotide exchange factor (GEF) Vav2 (Duan et al., 2010). The phenotype driven by Vav2 is dependent on activation of Rac1 and Cdc42. Given that overexpression of the p110β$^{SD/KA}$ mutant resulted in reduced AKT activation and failed to elicit the phenotype observed in MCF-10A cells overexpressing wild-type p110β, our data show that isoform-specific motile and invasive phenotype due to p110β expression is dependent on its association with Rac1.

Both *PIK3CB* and *RAC1* are amplified in a small proportion of breast cancers. While co-occurrence of *PIK3CB* and *RAC1* alterations

Journal of Cell Science (2021) 134, jcs248294. doi:10.1242/jcs.248294

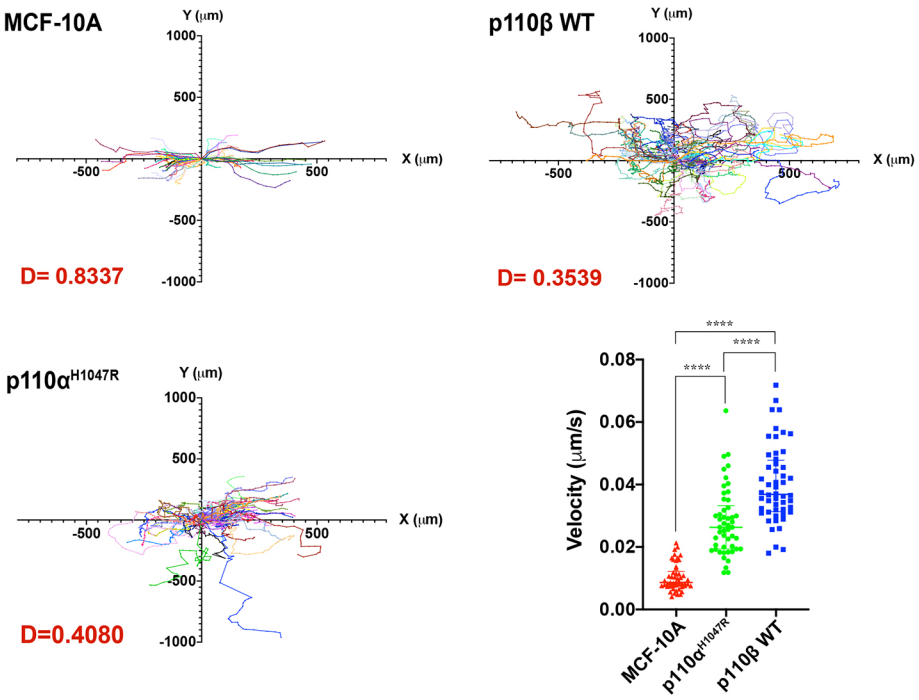

Fig. 7. p110β overexpression in MCF-10A cells results in loss of directionality, and increased motility. Cells were grown to confluency and a wound was formed in the cell monolayer, cell migration was observed over 8 h. Upper panels, cell trajectory of 50 cells over 8 h of migration, p110β and p110α^{H1047R} cells undergo loss of directional cell migration, depicted by the decreased directionality constant 'D' relative to parental MCF-10A cells. Lower panels, cell velocity of 50 cells over 8 h; p110β cells have significantly increased motility relative to p110α^{H1047R} and parental MCF-10A cells. Error bars show overall mean±s.e.m. of the velocity of the 50 cells across three independent experiments. ****P<0.0001 (one-way ANOVA with Tukey's analysis).

in breast cancers has Log2 Odds Ratio of 2.45 (P<0.022), these represent only three of the 130 characterized breast tumours with either *PIK3CB* or *RAC1* altered (90 tumours with *PIK3CB* alone; 37 tumours with *RAC1* alone). Significant exclusivity for *PIK3CB* and *RAC1* is observed, however, for lung cancers (Jordan et al., 2017), bladder cancers (Robertson et al., 2017), and head and neck squamous carcinoma (Hoadley et al., 2018). In the case of breast cancers, p110β expression is correlated with higher grade, increased rate of distant metastases and an overall more aggressive profile, concomitant with decreased overall patient survival (Carvalho et al., 2010). We propose that the signalling loop involving p110β and Rac1 may be a more general mechanism driving the invasive properties associated with p110β amplification, providing a potential avenue for development of therapeutic strategies targeting both p110β and Rac1 in invasive tumours with amplification of the *PIK3CB* gene.

MATERIALS AND METHODS

Cell lines and cell culture

MCF-10A cells were obtained from the American Type Culture Collection (Manassas, VA, USA) and cultured in growth medium containing DMEM/F12, 5% horse serum (HS), 1% penicillin and streptomycin, 20 ng/ml epidermal growth factor (EGF), 10 µg/ml insulin, 100 µg/ml hydrocortisone and 1 ng/ml cholera toxin. MCF-10A cells expressing the H1047R mutant of *PIK3CA* and wild-type *PIK3CB* were gifts from Dr Xiaolong Yang (Queens University, Kingston, Ontario, Canada) (Zhao et al., 2018). MCF-10A cells expressing wild-type *PIK3CA* were generated by retroviral gene transfer of pBabe-puro ^{HA}*PIK3CA* (Addgene #12522; Cambridge, MA, USA). MCF-10A cells expressing the *PIK3CB*$^{SD/KA}$ RBD mutant were generated by retroviral gene transfer of pBabe-puro *PIK3CB*$^{SD/KA}$. Where indicated, cells were cultured in MCF-10A medium in the absence of growth factors, EGF and insulin.

Small-molecule inhibitors

Wortmannin was obtained from Sigma-Aldrich (St Louis, Missouri, USA), and prepared as suggested by manufacturer, and used where indicated at various concentration and incubation times.

Western blot analyses and antibodies

Cell lysates were collected, and proteins were extracted in 1% NP-40 buffer (50 mM Tris-HCl pH 8.0, 120 mM NaCl, 1% NP-40) as described previously (Fleet and Hamel, 2018). For SDS-PAGE analyses, 50 µg cell lysate in 4× SDS loading dye (200 mM Tris-HCl pH 6.8, 8% SDS, 0.4% Bromophenol Blue, 40% glycerol and 400 mM β-mercaptoethanol) were incubated at 37°C for at least 20 min prior to separation on 10-12% SDS-PAGE. Separated proteins were electrophoretically transferred onto nitrocellulose membrane, blocked in 5% skim milk in phosphate buffered saline (PBS) for 1 h and then incubated overnight incubation with primary antibodies in PBS containing 3% BSA. Antibodies used were against phospho-Akt (Ser473) (1:1000, CST #9271; Danvers, MA, USA), total-Akt (1:1000, CST #4691), E-cadherin 4A2C7 (1:1000, Thermo Fisher 33-400), β-catenin (1:1000, CST #9562), Snail (C15D3) (1:1000, CST #3879), actin (1:1000), PI3K p110α (1:1000, CST # 4255), PI3K p110β (1:1000, CST #3011), Rac1 (BD Biosciences, 610650; Mississaugua, Ontario, Canada), GAPDH (Abcam, ab8245; Cambridge, UK) and lamin A/C (Santa Cruz Biotechnology, sc-376248; Dallas, TX, USA). The following day, membranes were incubated with HRP-conjugated secondary antibodies in 5% skim milk in PBS for 1 h [1:5000 goat anti-rabbit-IgG (CST #7074), or goat anti-mouse-IgG (CST 7076)). Blots were developed with Western Lightning PLUS ECL (PerkinElmer Life Sciences; Waltham, MA, USA) and imaged using a MicroChemi 2.0 Imager (FroggaBio; Toronto, Ontario, Canada).

Three-dimensional cell culture

MCF-10A cells were grown in 3D cultures on reconstituted basement membrane as previously described (Debnath et al., 2003). Briefly, 100% Matrigel™ (Corning; Corning, New York, US) was spread onto eight-well chamber slides and allowed to solidify. MCF-10A cells were seeded at 5.0×10^3 cells per well in assay medium supplemented with 2% HS, 5 ng/ml EGF and 2% Matrigel™ and all other components of the MCF-10A growth medium. Images of organoids were taken starting at day 3 post-seeding up to day 10. These images were acquired with a Nikon Eclipse TE2000-5 inverted microscope using the QICAM-UV Fast1394 camera (QImaging; Redwood City, California, US), and QCapture Suite PLUS software. Medium was changed every 4 days. After day 10, organoids were fixed in PBS with 2% PFA, and were probed for β-catenin to observe lateral membranes of cells with immunofluorescence as described below.

Immunofluorescence

Primary antibodies for β-catenin (1:200; CST, #9562), E-cadherin (1:200; Thermo Fisher, 33-400), Snail (1:500; CST, #3879) and β-tubulin along

Journal of Cell Science (2021) 134, jcs248294. doi:10.1242/jcs.248294

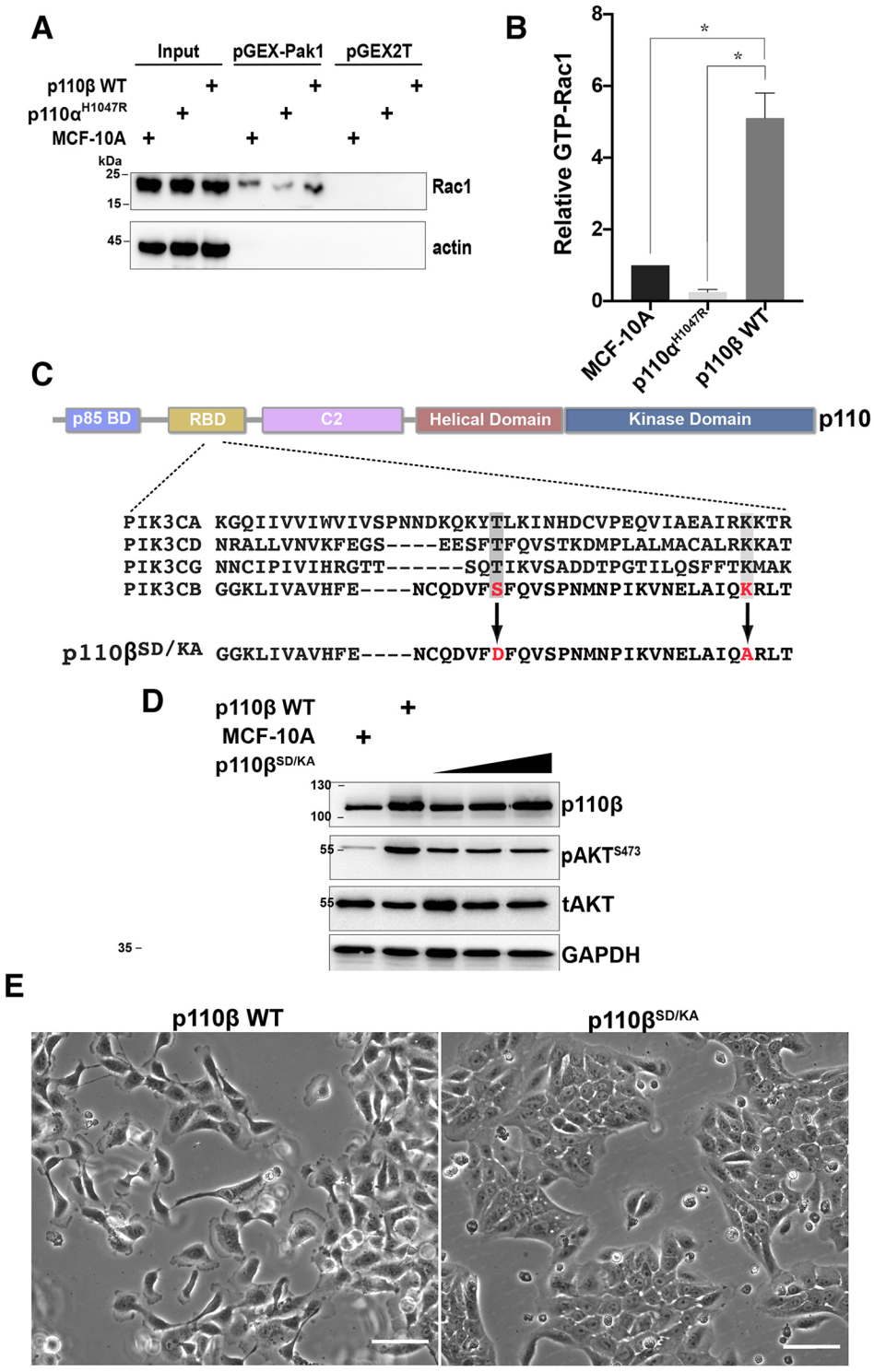

Fig. 8. Rac1 is necessary for the mesenchymal phenotype induced by overexpression of p110β during transformation of MCF-10A cells. Purified Pak1-bound GST beads were incubated with 250 µg of respective cell lysate. (A) Protein expression of GTP-Rac1, is significantly increased in p110β cells relative to $p110\alpha^{H1047R}$ and parental cell lines. (B) Quantification of GTP-Rac1 protein expression. Results are mean±s.e.m. of three independent experiments. *P<0.0332 (one-way ANOVA with Tukey's analysis). (C) The p110β S211D/K230A RBD mutant ($p110\beta^{SD/KA}$) abrogates binding of Rac1 to p110β. (D) Ectopic overexpression of $p110\beta^{SD/KA}$ in MCF-10A cells results in decreased activation of AKT relative to MCF-10A cells overexpressing wild-type p110β, as depicted by phosphorylation of Ser473 ($pAKT^{S473}$) in a representative western blot image. (E) $p110\beta^{SD/KA}$ mutant cells overexpressing MCF-10A do not invoke enhanced cell spreading and prominent lamellipodia formation as observed in wild-type *PIK3CB* overexpressing MCF-10A cells. Scale bars: 100 µm.

with a TRITC-conjugated phalloidin (1:200; Thermo Fisher, #A12380) were used for immunofluorescence staining in MCF-10A cells. Secondary antibodies used were donkey anti-rabbit-IgG conjugated to Alexa Fluor 488 (1:200; Invitrogen, #537118; Carlsbad, CA, USA) and donkey anti-mouse-IgG (1:200; Invitrogen, #A10037). All cells were plated on 12 mm glass coverslips, at densities indicated for individual experiments. Staining for adherens junction complexes and SNAIL in 2D cultures were undertaken as previously described (Fleet et al., 2016). Images were acquired with a Nikon Eclipse 80*i* fluorescence microscope using QICAM-UV Fast 1394 camera (QImaging), and QCapture Suite PLUS software, or confocal images were acquired with a ZEISS LSM 700 confocal microscope (Carl Zeiss Microscopy; Oberkochen, Germany) using the ZEISS ZEN microscope software.

Three-dimensional cultures were stained after 10–12 days. Organoids were stained as previously described (Debnath et al., 2003). In short, medium was removed from eight-well glass chamber slides, and organoids were washed once prior to fixation in freshly prepared 2% PFA in PBS for 20 min at room temperature. Organoids were then permeabilized in 0.5% Triton X-100 in PBS solution for 10 min at 4°C, prior to being rinsed with glycine solution (130 mM NaCl, 7 mM Na_2HPO_4, 3.5 mM NaH_2PO_4,

100 mM glycine in PBS) for 10 min at room temperature. Then they were incubated with primary antibody for β-catenin in immunofluorescence (IF) buffer (130 mM NaCl, 7 mM Na_2HPO_4, 3.5 mM NaH_2PO_4, 7.7 mM NaN_3, 0.1% BSA, 0.2% Triton X-100, 0.05% Tween-20 and 10% donkey serum in PBS) at the indicated concentrations overnight at 4°C. Primary antibody was removed and rinsed with IF buffer for 15 min at RT prior to incubation with secondary antibody in IF buffer for 1 h at room temperature in the dark. Secondary antibody was removed and organoids were rinsed with IF buffer at room temperature prior to mounting. Coverslips were mounted with Vectashield with DAPI (Vector Labs, #64335; Burlington, ON, Canada) and confocal immunofluorescence and *Z*-stack images were acquired with a ZEISS LSM 700 confocal microscope (Carl Zeiss Microscopy, Germany) using the ZEISS ZEN microscope software.

Wound migration assay

MCF-10A cells were plated on 12 mm glass coverslips at high confluency, in 12-well tissue culture plates. Cross sectional wounds were made, 24 h after plating, on coverslips using a P200 tip. Coverslips were then washed with PBS, and fresh complete medium was added to each well. Cells were stained with phalloidin and DAPI, as indicated above, to monitor movement until complete wound closure. Images were acquired using a Nikon Eclipse 80*i* fluorescence microscope using QICAM-UV Fast 1394 camera (QImaging), and QCapture Suite PLUS software. The percentage area left to cover during 7 h of wound closure was determined at each hour of migration for three independent experiments. ImageJ was used to calculate the area left uncovered by cells. This was done by using a rolling ball filter to correct the background, finding the edges of cells (Process Find Edges), using a Gaussian blur filter for noise reduction (Process>Filters>Guassian Blur), and adjusting the threshold to highlight all cells (Image>Adjust>Threshold). The area to measure was set (Analyze>Set Measurements) 'Area', and 'Limit to threshold' were selected. The percentage area was then measured (Analyze>Measure).

To determine cell trajectory, cells were plated and the wound was prepared as described above. Live-cell images were taken every 5 min to monitor cell movement over 7–8 h of wound closure with a VWR VistaVision upright compound microscope (VWR; Radnor, PA, USA) using the QICAM-UV Fast 1394 camera (QImaging) and QCapture Suite PLUS software. Analysis of cell trajectory was performed for 50 cells across three independent wound assays. ImageJ (National Institutes of Health, Bethesda, MD, USA) Manual Tracking Plugin was used to track XY coordinates of individual cells in 5 min frames (for *PIK3CB* and H1047R MCF-10A cells) and 15 min frames (for parental MCF-10A cells) over 7–8 h of migration. Cell trajectories for individual cells were mapped on rose plots, and the directionality constant was determined from the ratio between the Euclidian distance ($d_{euc;}$ length of straight line between cell start and endpoint) and total accumulated distance ($d_{acc;}$ in the cell path from start to endpoint) Eqn 1.

$$D = d_{euc}/d_{acc} \quad (1)$$

The average velocity of 50 individual cells across three independent wound assays over 7–8 h of migration was calculated by ratio between the average total accumulated distance of each cell and the duration of each assay in seconds.

RNA extraction and quantitative PCR

MCF-10A cell lines were plated in six-well plates in triplicate at 1.5×10^4 cells/well. After 24 h, cells were washed with PBS and medium was replaced with medium lacking growth factors for 48 h. Cells were collected in TRIzol® and total cellular RNA was extracted according to manufacturer's instructions. RNA was treated with DNase (Thermo Fisher, #EN0525) to remove residual genomic DNA, and 1 µg of RNA was incubated with 0.5 µM random primers prior to reverse transcription reactions using Superscript™ III Reverse Transcriptase (Invitrogen, #18080044) and treatment with RNase OUT (Invitrogen, #10777019) according to manufacturer's instructions. Generated cDNA samples were stored at −20°C until use. Quantitative PCR reactions were performed in a CFX384 Touch Real Time PCR Detection System (Bio-Rad, CA, USA). Primers for target genes were designed using Primer3 and are as follows: *CDH1*, (F) 5′- TCTCTCACGCTGTGTCATCC-'3, (R) 5′-ATTCGGGCT-TGTTGTCATTC-3′;

CDH2, (F) 5′-AGGATCAACCCCATACACCA-3′, (R) 5′-TGGTTTG-ACCACGGTGACTA-3′; *SNAI1*, (F) 5′-TTTACCTTCCAGCAGCCCTA-3′, (R) 5′-GGACAGAGTCCCAGATGAGC-3′; *GAPDH*, (F) 5′-CGTGG-AAGGACTCATGAC-3′, (R) 5′-AGGCAGGGATGATGTTCT-3′; *HA-PIK3CA*, (F) 5′-GTGCCAGATTACGCCAGATC-3′, (R) 5′-ACGGAGG-CATTCTAAAGTCACTA-3′; *PIK3CA*, (F) 5′- ACCTTGTTCCAATCCC-AGGT-3′, (R) 5′-ATGGAAAGGCAAAGTCGAGC-3′; and *PIK3CB*, (F) 5′- GGATGTTGCCTTATGGCTGT-3′, (R) 5′-CAGGTCATCCCCAGA-GTTGT-3′.

PCRs was performed using Sso Advanced Universal SYBR Green Mastermix (Bio-Rad; Hercules, CA, USA) in 10 µl reactions containing 5 pmol forward and reverse primer and 200 ng cDNA. Reaction conditions were an initial denaturation and polymerase activation at 95°C for 3 min, followed by 40 cycles for amplification at 95°C for 15 s, 60°C for 15 s, and 72°C for 30 s. Amplification was followed by a melt curve analysis. Data was retrieved using CFX Manager™ Software (Bio-Rad), and quantification to determine fold change relative to GAPDH as the endogenous control was done using the $2^{-\Delta\Delta CT}$ method.

GST protein purification and Rac activation assay

Cultures of *Escherichia coli* cells expressing the C-terminal portion of Pak1 bound to PGEXTK, and PGEX2T alone were grown until they reached an OD (at 600 nm) of 0.4–0.8 and then induced with 100 µM IPTG for 3 h until the OD_{600} reached between 2 and 4. Cultures were spun down at 5000 ***g*** at 4°C and resuspended in 1% NP-40 buffer (25 mM Tris-HCl pH 8.0, 150 mM NaCl, 5 mM $MgCl_2$, 5% Glycerol, 2 mM EDTA) supplemented with 5 µg/ml DNase, 20 µg/ml RNase A, 1 mg/ml lysozyme and 10 mM NaF, 1 mM PMSF, 1 mM Na_3VO_4, and 2 µg/ml leupeptin and aprotenin. Resuspended cells were incubated at 37°C for 1 h and subsequently spun down at 15,000 ***g*** at 4°C. GST fusion protein-containing supernatants were incubated with glutathione beads (Thermo Fisher, #16101) for 15 min, and washed three times in ice-cold NP-40 lysis buffer to remove unbound proteins. A fraction of the immobilized GST fusion proteins bound to glutathione beads were separated on 12% SDS-PAGE and gels were stained with Coomassie Brilliant Blue; 20 µg of GST or GST fusion proteins bound to beads were then used immediately in Rac1 activation assays.

For Rac1 activation assays, MCF-10A cells were seeded at 3×10^5 cells in 100 mm tissue culture plates, and collected after 48 h in 1% NP-40 lysis buffer. Samples were prepared with 350 µg of cellular lysate and 20 µg of isolated GST–Pak1 or GST alone on glutathione beads. Samples were incubated at 4°C for 1 h, unbound proteins collected and the bound protein was washed five times with ice-cold NP-40 buffer. For western analysis, 50 µg of total lysate (input) was run along with beads containing activated Rac1 bound to either GST–Pak1 or GST alone. Western blots were then prepared and probed for Rac1 as well as for actin as described above.

Cloning

To produce a retroviral vector expressing p110β with an S211D and K230A double mutation (SD/KA) in the RBD, the following gene was synthesized of the RBD in p110β: 5′-TTTGACTTTCAAGTGTCTCCTAATATGAA-TCCTATCAAAGTAAATGAATTGGCAATCCAAGCACGTTTGACTA-TTCATGGGAAGGAAGATGAAGTTAGCCCCTATGATTATGTGTTG-CAAGTCAGCGGGAGAGTAGAATATGTTTTTGGTGATCATCCACT-AATTCAGTTCCAGTATA- 3′.

The gene was synthesized with two flanking restriction enzyme sites for a 5′ BmgBI site, and 3′ BspEI site (Eurofins Genomics; Luxembourg). pBSF1-p110β (#34891, Addgene) was digested with BmgBI and BspEI, and the synthesized gene was inserted into the vector. The pBSF1- p110β SD/KA mutant synthesized was digested with EcoRV and SalI to cut out the p110β SD/KA gene, and ligated into the pBabe Puro retroviral backbone digested with compatible enzymes.

Acknowledgements

The authors thank Prof. X. Yang (Queen's University, Kingston, Ontario) for cell lines and Maya Latif for excellent technical assistance.

Competing interests
The authors declare no competing or financial interests.

Author contributions
Conceptualization: E.G., P.A.H.; Methodology: E.G., P.A.H.; Validation: E.G., P.A.H.; Formal analysis: E.G.; Investigation: E.G.; Resources: E.G., P.A.H.; Data curation: E.G.; Writing - original draft: E.G.; Writing - review & editing: E.G., P.A.H.; Visualization: E.G., P.A.H.; Supervision: P.A.H.; Project administration: E.G., P.A.H.; Funding acquisition: E.G., P.A.H.

Funding
This work was supported by a grant to P.A.H. (MOP-142490) from the Canadian Institutes of Health Research. E.G. was supported by a Canadian Institutes of Health Research Canada Graduate Scholarship-Masters (CIHR CGS-M).

Peer review history
The peer review history is available online at https://jcs.biologists.org/lookup/doi/10.1242/jcs.248294.reviewer-comments.pdf.

References

Akhtar, N. and Hotchin, N. A. (2001). RAC1 regulates Adherens junctions through endocytosis of E-Cadherin. *Mol. Biol. Cell* **12**, 847-862. doi:10.1091/mbc.12.4.847

Alan, J. K. and Lundquist, E. A. (2013). Mutationally activated Rho GTPases in cancer. *Small GTPases* **4**, 159-163. doi:10.4161/sgtp.26530

Bi, L., Okabe, I., Bernard, D. J., Wynshaw-Boris, A. and Nussbaum, R. L. (1999). Proliferative defect and embryonic lethality in mice homozygous for a deletion in the p110α subunit of phosphoinositide 3-kinase. *J. Biol. Chem.* **274**, 10963-10968. doi:10.1074/jbc.274.16.10963

Bi, L., Okabe, I., Bernard, D. J. and Nussbaum, R. L. (2002). Early embryonic lethality in mice deficient in the p110beta catalytic subunit of PI 3-kinase. *Mamm. Genome* **13**, 169-172. doi:10.1007/BF02684023

Cain, R. J. and Ridley, A. J. (2009). Phosphoinositide 3-kinases in cell migration. *Biol. Cell* **101**, 13-29. doi:10.1042/BC20080079

Cancer Genome Atlas Network (2012). Comprehensive molecular portraits of human breast tumours. *Nature* **490**, 61-70. doi:10.1038/nature11412

Cancer Genome Atlas Research Network (2011). Integrated genomic analyses of ovarian carcinoma. *Nature* **474**, 609-615. doi:10.1038/nature10166

Cancer Genome Atlas Research Network (2012). Comprehensive genomic characterization of squamous cell lung cancers. *Nature* **489**, 519-525. doi:10.1038/nature11404

Cancer Genome Atlas Research Network, **Kandoth, C., Schultz, N., Cherniack, A. D., Akbani, R., Liu, Y., Shen, H., Robertson, A. G., Pashtan, I., Shen, R.** (2013a). Integrated genomic characterization of endometrial carcinoma. *Nature* **497**, 67-73. doi:10.1038/nature12113

Cancer Genome Atlas Research Network, **Weinstein, J. N., Collisson, E. A., Mills, G. B., Shaw, K. R. M., Ozenberger, B. A., Ellrott, K., Shmulevich, I., Sander, C. and Stuart, J. M.** (2013b). The cancer genome atlas pan-cancer analysis project. *Nat. Genet.* **45**, 1113-1120. doi:10.1038/ng.2764

Carvalho, S., Milanezi, F., Costa, J. L., Amendoeira, I. and Schmitt, F. (2010). PIKing the right isoform: the emergent role of the p110β subunit in breast cancer. *Virchows Arch.* **456**, 235-243. doi:10.1007/s00428-010-0881-0

Ciraolo, E., Iezzi, M., Marone, R., Marengo, S., Curcio, C., Costa, C., Azzolino, O., Gonella, C., Rubinetto, C., Wu, H. et al. (2008). Phosphoinositide 3-kinase p110β activity: key role in metabolism and mammary gland cancer but not development. *Sci. Signal.* **1**, ra3. doi:10.1126/scisignal.1161577

Cizmecioglu, O., Ni, J., Xie, S., Zhao, J. J. and Roberts, T. M. (2016). Rac1-mediated membrane raft localization of PI3K/p110β is required for its activation by GPCRs or PTEN loss. *eLife* **5**, e17635. doi:10.7554/eLife.17635

Coffer, P. J., Jin, J. and Woodgett, J. R. (1998). Protein kinase B (c-Akt): a multifunctional mediator of phosphatidylinositol 3-kinase activation. *Biochem. J.* **335**, 1-13. doi:10.1042/bj3350001

Dbouk, H. A., Pang, H., Fiser, A. and Backer, J. M. (2010). A biochemical mechanism for the oncogenic potential of the p110β catalytic subunit of phosphoinositide 3-kinase. *Proc. Natl. Acad. Sci. USA* **107**, 19897. doi:10.1073/pnas.1008739107

Dbouk, H. A., Vadas, O., Shymanets, A., Burke, J. E., Salamon, R. S., Khalil, B. D., Barrett, M. O., Waldo, G. L., Surve, C., Hsueh, C. et al. (2012). G protein–coupled receptor–mediated activation of p110β by Gβγ is required for cellular transformation and invasiveness. *Sci. Signal.* **5**, ra89-ra89. doi:10.1126/scisignal.2003264

Debnath, J., Muthuswamy, S. K. and Brugge, J. S. (2003). Morphogenesis and oncogenesis of MCF-10A mammary epithelial acini grown in three-dimensional basement membrane cultures. *Methods* **30**, 256-268. doi:10.1016/S1046-2023(03)00032-X

Downes, C. P. and Carter, A. N. (1991). Phosphoinositide 3-kinase: a new effector in signal transduction? *Cell. Signal.* **3**, 501-513. doi:10.1016/0898-6568(91)90027-R

Duan, L., Chen, G., Virmani, S., Ying, G. G., Raja, S. M., Chung, B. M., Rainey, M. A., Dimri, M., Ortega-Cava, C. F., Zhao, X. et al. (2010). Distinct roles for Rho versus Rac/Cdc42 GTPases downstream of Vav2 in regulating mammary epithelial acinar architecture. *J. Biol. Chem.* **285**, 1555-1568. doi:10.1074/jbc.M109.057976

Elisha, Y., Kalchenko, V., Kuznetsov, Y. and Geiger, B. (2018). Dual role of E-cadherin in the regulation of invasive collective migration of mammary carcinoma cells. *Sci. Rep.* **8**, 4986. doi:10.1038/s41598-018-22940-3

Feigin, M. E. and Muthuswamy, S. K. (2009). Polarity proteins regulate mammalian cell-cell junctions and cancer pathogenesis. *Curr. Opin. Cell Biol.* **21**, 694-700. doi:10.1016/j.ceb.2009.07.003

Fleet, A. J. and Hamel, P. A. (2018). The protein-specific activities of the transmembrane modules of Ptch1 and Ptch2 are determined by their adjacent protein domains. *J. Biol. Chem.* **293**, 16583-16595. doi:10.1074/jbc.RA118.004478

Fleet, A., Lee, J. P. Y., Tamachi, A., Javeed, I. and Hamel, P. A. (2016). Activities of the cytoplasmic domains of patched-1 modulate but are not essential for the regulation of canonical hedgehog signaling. *J. Biol. Chem.* **291**, 17557-17568. doi:10.1074/jbc.M116.731745

Fritsch, R., de Krijger, I., Fritsch, K., George, R., Reason, B., Kumar, M. S., Diefenbacher, M., Stamp, G. and Downward, J. (2013). RAS and RHO families of GTPases directly regulate distinct phosphoinositide 3-kinase isoforms. *Cell* **153**, 1050-1063. doi:10.1016/j.cell.2013.04.031

Fritz, G., Just, I. and Kaina, B. (1999). Rho GTPases are over-expressed in human tumors. *Int. J. Cancer* **81**, 682-687. doi:10.1002/(SICI)1097-0215(19990531)81:5<682::AID-IJC2>3.0.CO;2-B

Fritz, G., Brachetti, C., Bahlmann, F., Schmidt, M. and Kaina, B. (2002). Rho GTPases in human breast tumours: expression and mutation analyses and correlation with clinical parameters. *Br. J. Cancer* **87**, 635-644. doi:10.1038/sj.bjc.6600510

Gabelli, S. B., Mandelker, D., Schmidt-Kittler, O., Vogelstein, B. and Amzel, L. M. (2010). Somatic mutations in PI3Kα: structural basis for enzyme activation and drug design. *Biochim. Biophys. Acta (BBA) Proteins and Proteomics* **1804**, 533. doi:10.1016/j.bbapap.2009.11.020

Guillermet-Guibert, J., Bjorklof, K., Salpekar, A., Gonella, C., Ramadani, F., Bilancio, A., Meek, S., Smith, A. J. H., Okkenhaug, K. and Vanhaesebroeck, B. (2008). The p110β isoform of phosphoinositide 3-kinase signals downstream of G protein-coupled receptors and is functionally redundant with p110γ. *Proc. Natl. Acad. Sci. USA* **105**, 8292-8297. doi:10.1073/pnas.0707761105

Hoadley, K. A., Yau, C., Wolf, D. M., Cherniack, A. D., Tamborero, D., Ng, S., Leiserson, M. D. M., Niu, B., McLellan, M. D., Uzunangelov, V. et al. (2014). Multiplatform analysis of 12 cancer types reveals molecular classification within and across tissues of origin. *Cell* **158**, 929-944. doi:10.1016/j.cell.2014.06.049

Hoadley, K. A., Yau, C., Hinoue, T., Wolf, D. M., Lazar, A. J., Drill, E., Shen, R., Taylor, A. M., Cherniack, A. D., Thorsson, V. et al. (2018). Cell-of-origin patterns dominate the molecular classification of 10,000 tumors from 33 types of cancer. *Cell* **173**, 291-304.e6. doi:10.1016/j.cell.2018.03.022

Huang, R. Y.-J., Guilford, P. and Thiery, J. P. (2012). Early events in cell adhesion and polarity during epithelial-mesenchymal transition. *J. Cell Sci.* **125**, 4417-4422. doi:10.1242/jcs.099697

Isakoff, S. J., Engelman, J. A., Irie, H. Y., Luo, J., Brachmann, S. M., Pearline, R. V., Cantley, L. C. and Brugge, J. S. (2005). Breast cancer–associated PIK3CA mutations are oncogenic in mammary epithelial cells. *Cancer Res.* **65**, 10992-11000. doi:10.1158/0008-5472.CAN-05-2612

Jordan, E. J., Kim, H. R., Arcila, M. E., Barron, D., Chakravarty, D., Gao, J. J., Chang, M. T., Ni, A., Kundra, R., Jonsson, P. et al. (2017). Prospective comprehensive molecular characterization of lung adenocarcinomas for efficient patient matching to approved and emerging therapies. *Cancer Discov.* **7**, 596-609. doi:10.1158/2159-8290.CD-16-1337

Kang, S., Denley, A., Vanhaesebroeck, B. and Vogt, P. K. (2006). Oncogenic transformation induced by the p110β, -γ, and -δ isoforms of class I phosphoinositide 3-kinase. *Proc. Natl. Acad. Sci. USA* **103**, 1289. doi:10.1073/pnas.0510772103

Kazlauskas, A. (1994). Receptor tyrosine kinases and their targets. *Curr. Opin. Genet. Dev.* **4**, 5-14. doi:10.1016/0959-437X(94)90085-X

Keely, P. J., Westwick, J. K., Whitehead, I. P., Der, C. J. and Parise, L. V. (1997). Cdc42 and Rac1 induce integrin-mediated cell motility and invasiveness through PI(3)K. *Nature* **390**, 632-636. doi:10.1038/37656

Knights, A. J., Funnell, A. P. W., Crossley, M. and Pearson, R. C. M. (2012). Holding tight: cell junctions and cancer spread. *Trends Cancer Res.* **8**, 61-69.

Lamouille, S., Xu, J. and Derynck, R. (2014). Molecular mechanisms of epithelial–mesenchymal transition. *Nat. Rev. Mol. Cell Biol.* **15**, 178-196. doi:10.1038/nrm3758

Larue, L. and Bellacosa, A. (2005). Epithelial–mesenchymal transition in development and cancer: role of phosphatidylinositol 3′ kinase/AKT pathways. *Oncogene* **24**, 7443-7454. doi:10.1038/sj.onc.1209091

Le Bras, G. F., Taubenslag, K. J. and Andl, C. D. (2012). The regulation of cell-cell adhesion during epithelial-mesenchymal transition, motility and tumor progression. *Cell Adhes. Migr.* **6**, 365-373. doi:10.4161/cam.21326

Macara, I. G. and McCaffrey, L. (2013). Cell polarity in morphogenesis and metastasis. *Phil. Trans. R. Soc. B* **368**, 20130012. doi:10.1098/rstb.2013.0012
Manning, B. D. and Toker, A. (2017). AKT/PKB signaling: navigating the network. *Cell* **169**, 381-405. doi:10.1016/j.cell.2017.04.001
Muqbil, I., Wu, J., Aboukameel, A., Mohammad, R. M. and Azmi, A. S. (2014). Snail nuclear transport: the gateways regulating epithelial-to-mesenchymal transition? *Semin. Cancer Biol.* **27**, 39-45. doi:10.1016/j.semcancer.2014.06.003
Nieto, M. A. (2002). The snail superfamily of zinc-finger transcription factors. *Nat. Rev. Mol. Cell Biol.* **3**, 155-166. doi:10.1038/nrm757
Nobes, C. and Hall, A. (1994). Regulation and function of the Rho subfamily of small GTPases. *Curr. Opin. Genet. Dev.* **4**, 77-81. doi:10.1016/0959-437X(94)90094-9
Pawson, T., Olivier, P., Rozakis-Adcock, M., McGlade, J. and Henkemeyer, M. (1993). Proteins with SH2 and SH3 domains couple receptor tyrosine kinases to intracellular signalling pathways. *Phil. Trans. R. Soc. B* **340**, 279-285. doi:10.1098/rstb.1993.0069
Pereira, B., Chin, S.-F., Rueda, O. M., Vollan, H.-K. M., Provenzano, E., Bardwell, H. A., Pugh, M., Jones, L., Russell, R., Sammut, S.-J. et al. (2016). The somatic mutation profiles of 2,433 breast cancers refine their genomic and transcriptomic landscapes. *Nat. Commun.* **7**, 11479. doi:10.1038/ncomms11479
Ridley, A. J. (2004). Rho proteins and cancer. *Breast Cancer Res. Treat.* **84**, 13-19. doi:10.1023/B:BREA.0000018423.47497.c6
Ridley, A. J. (2015). Rho GTPase signalling in cell migration. *Curr. Opin. Cell Biol.* **36**, 103-112. doi:10.1016/j.ceb.2015.08.005
Robertson, A. G., Kim, J., Al-Ahmadie, H., Bellmunt, J., Guo, G., Cherniack, A. D., Hinoue, T., Laird, P. W., Hoadley, K. A., Akbani, R. et al. (2017). Comprehensive molecular characterization of muscle-invasive bladder cancer. *Cell* **171**, 540-556.e25. doi:10.1016/j.cell.2017.09.007
Samuels, Y. and Velculescu, V. E. (2004). Oncogenic mutations of PIK3CA in human cancers. *Cell Cycle* **3**, 1221-1224. doi:10.4161/cc.3.10.1164
Shibasaki, F., Homma, Y. and Takenawa, T. (1991). Two types of phosphatidylinositol 3-kinase from bovine thymus. Monomer and heterodimer form. *J. Biol. Chem.* **266**, 8108-8114. doi:10.1016/S0021-9258(18)92948-0
Singh, P., Dar, M. S. and Dar, M. J. (2016). p110α and p110β isoforms of PI3K signaling: are they two sides of the same coin? *FEBS Lett.* **590**, 3071-3082. doi:10.1002/1873-3468.12377
Tojkander, S., Gateva, G. and Lappalainen, P. (2012). Actin stress fibers - assembly, dynamics and biological roles. *J. Cell Sci.* **125**, 1855-1864. doi:10.1242/jcs.098087
Thorpe, L. M., Yuzugullu, H. and Zhao, J. J. (2015). PI3K in cancer: divergent roles of isoforms, modes of activation and therapeutic targeting. *Nat. Rev. Cancer* **15**, 7-24. doi:10.1038/nrc3860
Utermark, T., Rao, T., Cheng, H., Wang, Q., Lee, S. H., Wang, Z. C., Iglehart, J. D., Roberts, T. M., Muller, W. J. and Zhao, J. J. (2012). The p110α and p110β isoforms of PI3K play divergent roles in mammary gland development and tumorigenesis. *Genes Dev.* **26**, 1573-1586. doi:10.1101/gad.191973.112
Vanhaesebroeck, B., Leevers, S. J., Panayotou, G. and Waterfield, M. D. (1997). Phosphoinositide 3-kinases: a conserved family of signal transducers. *Trends Biochem. Sci.* **22**, 267-272. doi:10.1016/S0968-0004(97)01061-X
Wee, S., Wiederschain, D., Maira, S.-M., Loo, A., Miller, C., deBeaumont, R., Stegmeier, F., Yao, Y.-M. and Lengauer, C. (2008). PTEN-deficient cancers depend on PIK3CB. *Proc. Natl. Acad. Sci. USA* **105**, 13057. doi:10.1073/pnas.0802655105
Yuzugullu, H., Baitsch, L., Von, T., Steiner, A., Tong, H., Ni, J., Clayton, L. K., Bronson, R., Roberts, T. M., Gritsman, K. et al. (2015). A PI3K p110β–Rac signalling loop mediates Pten-loss-induced perturbation of haematopoiesis and leukaemogenesis. *Nat. Commun.* **6**, 8501. doi:10.1038/ncomms9501
Zhang, X., Vadas, O., Perisic, O., Anderson, K. E., Clark, J., Hawkins, P. T., Stephens, L. R. and Williams, R. L. (2011). Structure of Lipid Kinase p110β/p85β Elucidates an unusual SH2-domain-mediated inhibitory mechanism. *Mol. Cell* **41**, 567-578. doi:10.1016/j.molcel.2011.01.026
Zhang, J., Gao, X., Schmit, F., Adelmant, G., Eck, M. J., Marto, J. A., Zhao, J. J. and Roberts, T. M. (2017). CRKL mediates p110β-dependent PI3K signaling in PTEN-deficient cancer cells. *Cell Rep.* **20**, 549-557. doi:10.1016/j.celrep.2017.06.054
Zhao, Y., Montminy, T., Azad, T., Lightbody, E., Hao, Y., SenGupta, S., Asselin, E., Nicol, C. and Yang, X. (2018). PI3K positively regulates YAP and TAZ in mammary tumorigenesis through multiple signaling pathways. *Mol. Cancer Res.* **16**, 1046-1058. doi:10.1158/1541-7786.MCR-17-0593
Zhou, B. P., Deng, J., Xia, W., Xu, J., Li, Y. M., Gunduz, M. and Hung, M.-C. (2004). Dual regulation of snail by GSK-3β-mediated phosphorylation in control of epithelial–mesenchymal transition. *Nat. Cell Biol.* **6**, 931-940. doi:10.1038/ncb1173